Since January 2020 Elsevier has created a COVID-19 resource centre with free information in English and Mandarin on the novel coronavirus COVID-19. The COVID-19 resource centre is hosted on Elsevier Connect, the company's public news and information website.

Chemico-Biological Interactions 334 (2021) 109300

Contents lists available at ScienceDirect

Chemico-Biological Interactions

journal homepage: www.elsevier.com/locate/chembioint

Plant isoquinoline alkaloids as potential neurodrugs: A comparative study of the effects of benzo[*c*]phenanthridine and berberine-based compounds on β-amyloid aggregation

Daniela Marasco [a,b,1], Caterina Vicidomini [b,1], Pawel Krupa [c,1], Federica Cioffi [d], Pham Dinh Quoc Huy [c], Mai Suan Li [c,e], Daniele Florio [a], Kerensa Broersen [f], Maria Francesca De Pandis [g], Giovanni N. Roviello [b,*]

[a] *Department of Pharmacy, University of Naples Federico II, Via Mezzocannone 16, 80134, Naples, Italy*
[b] *Istituto di Biostrutture e Bioimmagini IBB - CNR, Via Mezzocannone 16, I-80134 Naples, Italy*
[c] *Institute of Physics Polish Academy of Sciences, Al. Lotników 32/46, 02-668, Warsaw, Poland*
[d] *Nanobiophysics Group, Technical Medical Centre, Faculty of Science and Technology, University of Twente, Enschede, the Netherlands*
[e] *Institute for Computational Sciences and Technology, SBI building, Quang Trung Software City, Tan ChanhHiep Ward, District 12, Ho Chi Minh City, Viet Nam*
[f] *Applied Stem Cell Technologies, Technical Medical Centre, Faculty of Science and Technology, University of Twente, Enschede, the Netherlands*
[g] *San Raffaele Cassino Institute, San Raffaele SPA, 03043, Cassino, FR, Italy*

ARTICLE INFO

Keywords:
Amyloid beta
Neurodrug
Amyloid aggregation
Alzheimer's disease
Chelerythrine
Sanguinarine
Coralyne
Berberine

ABSTRACT

Herein we present a comparative study of the effects of isoquinoline alkaloids belonging to benzo[*c*]phenanthridine and berberine families on β-amyloid aggregation. Results obtained using a Thioflavine T (ThT) fluorescence assay and circular dichroism (CD) spectroscopy suggested that the benzo[*c*]phenanthridine nucleus, present in both sanguinarine and chelerythrine molecules, was directly involved in an inhibitory effect of $A\beta_{1-42}$ aggregation. Conversely, coralyne, that contains the isomeric berberine nucleus, significantly increased propensity for $A\beta_{1-42}$ to aggregate. Surface Plasmon Resonance (SPR) experiments provided quantitative estimation of these interactions: coralyne bound to $A\beta_{1-42}$ with an affinity ($K_D = 11.6\,\mu M$) higher than benzo[*c*]phenanthridines. Molecular docking studies confirmed that all three compounds are able to recognize $A\beta_{1-42}$ in different aggregation forms suggesting their effective capacity to modulate the $A\beta_{1-42}$ self-recognition mechanism. Molecular dynamics simulations indicated that coralyne increased the β-content of $A\beta_{1-42}$, in early stages of aggregation, consistent with fluorescence-based promotion of the $A\beta_{1-42}$ self-recognition mechanism by this alkaloid. At the same time, sanguinarine induced $A\beta_{1-42}$ helical conformation corroborating its ability to delay aggregation as experimentally proved *in vitro*. The investigated compounds were shown to interfere with aggregation of $A\beta_{1-42}$ demonstrating their potential as starting leads for the development of therapeutic strategies in neurodegenerative diseases.

1. Introduction

Several neurodegenerative disorders, including Alzheimer's (AD), Parkinson's (PD) and Huntington's (HD) diseases are associated with aggregation of misfolded proteins [1,2]. Among these, AD, a predominant cause of dementia worldwide [3,4], is characterized by extracellular amyloid deposits, whose main component is the 42-amino acid amyloid β peptide ($A\beta_{1-42}$), and by intracellular neurofibrillary tangles composed of tau [5,6].

$A\beta_{1-42}$ is a peptide cleaved from the amyloid precursor protein (APP), comprised of a charged *N*-terminal segment (amino acids 1–22), a hydrophobic central region (KLVFFA, amino acids 16–21), which alone is able to aggregate into insoluble fibrils, and a hydrophobic *C*-terminal region (residues 23–42). Once released as a monomer from APP into the extracellular space, $A\beta_{1-42}$ undergoes a structural transition gaining β-sheet content, and tends to aggregate into oligomeric, protofibrillar and fibrillar species [7]. $A\beta_{1-42}$ oligomeric assemblies have been related to AD pathogenesis for their role in neuronal damage and

* Corresponding author.
E-mail addresses: giroviel@unina.it, giovanni.roviello@cnr.it (G.N. Roviello).
[1] These authors equally contributed to this work.

https://doi.org/10.1016/j.cbi.2020.109300
Received 23 July 2020; Received in revised form 17 September 2020; Accepted 21 October 2020
Available online 22 October 2020

neurotoxicity following $A\beta_{1-42}$ aggregation [8]. In this context, preventing $A\beta_{1-42}$ aggregation with small molecules is one of the prominent strategies for the development of new therapies for AD [9–11]. To this scope, several plant extracts and natural products, such as curcumin, epigallocatechin-3-gallate, and resveratrol, were evaluated with promising results [12–14].

Isoquinoline alkaloids (Fig. 1) belong to one of the most complex families of plant alkaloids. They are nitrogenous metabolites distributed in many botanical families investigated nowadays for their significant biomedical importance [15–17]. Among these, benzo[*c*]phenanthridines and protoberberines are found in various vegetal sources belonging to the *Rutaceae* family (in particular from the *Zanthoxylum* genus [18]), with berberine (Fig. 1) being an interesting candidate for PD and AD thanks to multi-faceted defensive mechanisms and bio-molecular pathways involving this alkaloid [19,20]. However, its use as a neurodrug is hampered by its cytotoxic effects at relatively high concentration [21]. Hence, a structurally modified version of berberine that results in the nontoxic, free hydroxyl-bearing Ber-D was prepared, which was found to inhibit the aggregation and cell toxicity of $A\beta_{1-42}$ *in vitro* [22]. The berberine nucleus in Ber-D comprises four rings, of which three aromatic, whereas the anti-leukemic berberine-like drug coralyne (here indicated as CO, Fig. 1) contains all four aromatic rings [23,24].

Other examples of plant isoquinoline alkaloids are sanguinarine (SA) and chelerythrine (CH, Fig. 1), two tetracyclic aromatic compounds isolated from *Macleaya cordata* belonging to the family of benzo[*c*] phenanthridines, and also classifiable as azachrysenes [25,26]. In particular, SA is endowed with several properties of therapeutic relevance, including the reduction of levels of stress hormone as shown in studies carried out in animal models [27], as well as of serum haptoglobin, and serum amyloid A (SAA) [27,28]. This latter is mainly produced in the liver but also expressed extrahepatically in the central nervous system (CNS) [29], with increased levels in AD patients [29], and it was recently recognized as a biomarker for COVID-19 [30], that is a recently-emerged viral disease causing severe acute respiratory syndrome and diverse injuries in other systems [31–34]. SA and CH are believed to possess potential as neurodrugs for AD due to their ability to inhibit several neuropathologically-relevant enzymes [35]. However, clues of neuroprotective properties were found experimentally only for CH which inhibited *in vitro* amyloid aggregation [36], whereas the same inhibitory activity, predicted *in silico* for SA by some of us [37], had not been validated before on an experimental basis.

Thus, the scope of this work was to investigate the interaction between tetracyclic aromatic structures endowed with benzo[*c*]phenanthridine (SA, CH) and berberine (CO, Fig. 1) nuclei, respectively, with $A\beta_{1-42}$ peptide, by means of ThT fluorescence and CD spectroscopy to evaluate their effects on the aggregation of $A\beta_{1-42}$, and by surface plasmon resonance (SPR) assays to characterize these interactions.

Experimental data were further corroborated by *in silico* studies, through molecular docking simulations, to unveil preferential binding modes of ligands to different aggregated forms of $A\beta_{1-42}$, and by molecular dynamics simulations to explore the effects of these compounds in early aggregation stages of $A\beta_{1-42}$.

2. Materials and methods

2.1. Chemicals

$A\beta_{1-42}$ peptide (for CD and SPR), SA, CH, SA isoquinoline alkaloids and all other chemicals and solvents were purchased from Sigma-Aldrich (Amsterdam, The Netherlands). $A\beta_{1-42}$ peptide for ThT assay was purchased from rPeptide (GA, USA).

2.2. $A\beta_{1-42}$ peptide solubilization

Solutions of recombinant $A\beta_{1-42}$ peptide were prepared according to a previously published procedure [38]. In short, $A\beta_{1-42}$ was sequentially dissolved in hexafluoroisopropanol (HFIP) and DMSO. The DMSO was removed from the $A\beta_{1-42}$ solution by using a HiTrap™ desalting column (GE Healthcare, Zwijndrecht, The Netherlands) and elution with PBS at pH 7.4. We measured the $A\beta_{1-42}$concentration by the Coomassie (Bradford, UK) Protein Assay Kit (ThermoFisher, Landsmeer, The Netherlands) and, afterwards, the final concentration required for the subsequent experiments was achieved by dilution. Aβ peptide aggregation, in the presence or absence of SA, CH and CO, was evaluated at 37 °C under quiescent conditions.

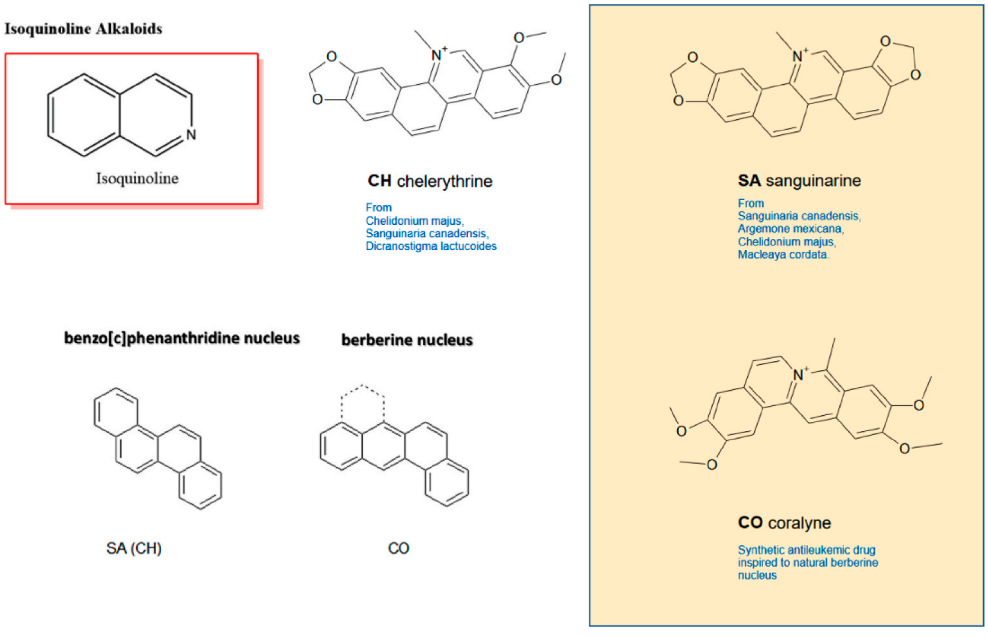

Fig. 1. The isoquinoline alkaloids of synthetic (CO) and plant (CH and SA) origin investigated in this work. All share an isoquinoline core (up, left) but are based on two different polycycle rearrangements (bottom, left).

2.3. Thioflavin-T assay

Aggregation was measured by a ThT fluorescence assay. The $A\beta_{1-42}$ concentration was adjusted to 25 μM using PBS buffer (pH 7.4), while a final ThT concentration of 12 μM was realized in a 96-well plate (Greiner flat bottom transparent black, Sigma–cat. M9685). Fluorescence intensity was measured at 37 °C using an automated well-plate reader (Tecan Infinite 200 PRO) at an excitation wavelength of 450 nm and emission detection from 480 to 600 nm. The fluorescence intensity from ThT at its maximum value (485 nm) was reported in a graph for the three complexes with the ligands (C = 25 μM). Measurements were performed in triplicate, the values recorded were averaged and background measurements that corresponded to buffer containing 12 μM ThT and the tested isoquinoline alkaloids subtracted. Measurements were performed after incubation for 2 h to allow Aβ to aggregate.

2.4. CD experiments

The CD experiments were conducted as previously described [39–53]. The spectra were obtained using a JascoJ-715 spectropolarimeter coupled to a PTC-348WI temperature control system, and a quartz cell with a path length of 1 cm, at 37 °C with a response of 1 s, a scanning speed of 100 nm/min and a 2.0 nm bandwidth. All the spectra were averaged over three scans. Experiments were carried out using a 5 μM concentration of $A\beta_{1-42}$ in PBS (overall volume = 2 ml, pH 7.2) and a twofold concentration of ligands. Spectra were collected after incubation at 37 °C for 0.5, 24 and 48 h.

2.5. Surface plasmon resonance (SPR) experiments

Surface plasmon resonance (SPR) binding assays were performed on a Biacore 3000 (GE Healthcare). $A\beta_{1-42}$ peptide was immobilized on a CM5 chip through an amine coupling procedure at 100 μg/mL in 10 mM sodium acetate (pH 4) at 2 μL/min until reaching an immobilization level of ~400 RU. Binding assays were carried out by injecting 90 μL of analyte, at 20 $\mu L/min^{-1}$. Experiments were carried out using PBS as running buffer. The association phase (k_{on}) was followed for 270 s, whereas the dissociation phase (k_{off}) was followed for 300 s. The reference chip sensorgrams were subtracted from sample sensorgrams. After each cycle, the sensor chip surface was regenerated with a 10 mM NaOH solution for 30 s. Analyte concentrations were for cheletrine 20, 40, 80 and 100 μM, sanguinarine 100, 300, 500, 700, 900 and 1100 μM and for coralyne 5, 20, 30, 40, 50, 70 μM. Experiments were carried out in duplicates. Kinetic parameters were estimated assuming a 1:1 binding model and using version 4.1 Evaluation Software (GE Healthcare).

2.6. In silico studies

In all computational studies, as initial $A\beta_{1-42}$ conformations we utilized S-shape and U-shape fibril models (PDB codes: 2LMN and 2MXU) and three of the most representative monomeric models from previous extensive computational studies [54].

2.7. Ligand parameterization

Fully-protonated structures of the three compounds (CO, SA, CH) were optimized by gaussian 09 software [55], utilizing Hartree-Fock method and 6-31G* basis set. AM1-BCC method [56] implemented in the AmberTools 19 package was used to derive charges of all atoms. Parameters for bonds, valence and dihedral angles were adapted from General Amber Force Field [57] based on structural similarity.

2.8. Docking

Global molecular docking of compounds to the monomeric, tetrameric, and fibrillar structures of $A\beta_{1-42}$ was performed using AutoDock 4.2.6 software [58] allowing flexibility of the ligand with rigid conformation of the receptor due to computational limitations. The algorithm was set to generate 100 initial docking positions and subsequently perform clustering using 10, 15, and 15 Å criteria for monomeric, tetrameric, and fibril structures, respectively, to obtain most probable docking positions (modes) of the compounds. Two different cutoff values were used due to large size differences between monomeric and other systems. AutoDock 4.2 was selected for docking, because it was found to provide more reliable binding energies than AutoDock Vina in recent studies [59]. In general, AutoDock 4.2.6 should provide reliable docking poses and estimated binding energies [60]. It should be mentioned that in all computational methods using approximate system representation, such as molecular docking or MD simulations, relative energies, rather than absolute should be analyzed, treating the latter with large possible error [61], however, usually binding energy stronger than −9 kcal/mol is treated as strong binding [62].

2.9. Molecular dynamics simulations

Two series of molecular dynamics (MD) simulations were performed: (i) fibrillar structures with the compounds bound to them, obtained through docking procedure, and (ii) 16 non-bound semi-extended $A\beta_{1-42}$ chains in the presence and absence of compounds. MD simulations of fibrillar $A\beta_{1-42}$ with compounds were performed using Amber ff14sb [63] force field with TIP3P water model [64], which should provide reliable results for these systems. Due to computational restrictions, MD simulations were performed for top 2 binding modes of each system, each of 10 separate trajectories, reaching in total 1 μs for each of the binding modes.

For MD simulations of 16 chains, we used an in-house algorithm to put pre-generated semi-extended $A\beta_{1-42}$ chains of random conformations as close to each other as possible, with the restriction to keep minimum distance of 8 Å between any heavy atoms of different chains to avoid possible bias coming from initial orientation of the chains. Such system was hydrated by adding approximately 47500 water molecules and charge was neutralized by inserting counterions, resulting in truncated octahedron boxes of total volume of approximately 1800 nm^3 resulting in total Aβ1-42 concentration of approximately 1 cM, which is order of magnitude higher than in other studies [65,66], yet still not in glass phase [67]. In simulations with compounds, small molecules were placed between $A\beta_{1-42}$ chains using the same criterion. In all simulations, initial orientations of $A\beta_{1-42}$ chains and compounds were identical.

Obtained systems were energy minimized, using steepest descent and conjugate gradient algorithm and equilibrated for 1ns. For each type of system, two trajectories were run, each of 800ns and then recorded 20,000 snapshots from the last 200 ns (600–800ns) were analyzed. To better capture aggregation effects in simulations of systems containing 16 chains, we utilized state-of-the-art Amber ff19sb force field [68] coupled with OPC water model [69], which should provide reliable results, especially for binding-dissociation process. Analysis of these simulations included root-mean-square deviation (RMDd) using initial structure as a reference, radius of gyration (Rg), solvent-accessible surface area (SASA) using LCPO method [70] and secondary structure determinations with DSSP [71] algorithm implemented into Amber19 package and various distance calculations. Distance criterion of 6.5 Å between centers of mass of two side-chains was used to determine a contact between chains, and a criterion of 5 contacts was used to determine the size of the oligomer (e.g. two chains have to form at least 5 contacts to be named as dimer), as in our previous work [66] to discard structures forming weak interaction due to accidental proximity of the chains.

2.10. Molecular mechanics - Poisson Boltzmann Surface Area (MM/PBSA) method

MM-PBSA is a post-processing method which was used to calculate

the free energy difference, ΔG_{bind}, between the free and bound states of a molecule complex: receptor and ligand. ΔG_{bind} is calculated for a set of selective snapshots from simulation trajectory and is defined as follows:

$$\Delta G_{bind} = \Delta E_{elec} + \Delta E_{vdW} + \Delta E_{SUR} + \Delta E_{PB} - T\Delta S, \quad (1)$$

where ΔE_{elec} and ΔE_{vdW} are differences in electrostatic and van der Waals energy components, respectively, ΔE_{SUR} and ΔE_{PB} describe differences in non-polar and polar solvation free energies, respectively, and $T\Delta S$ represents the entropic contribution.

In this study, MM/PBSA methods implemented into the AmberTools 19 package was used to estimate ΔG_{bind} of compounds to fibrillar models using second halves of performed MD simulations. As a standard procedure, for energy calculation in MM/PBSA procedure we used the same force field adopted to perform the simulations, however, without cutoff for electrostatic and van der Waals interactions. The entropic term, $T\Delta S$, was estimated by normal mode approximation method, where ΔE_{PB} was obtained by solving numerically linearized Poisson-Boltzmann equation and ΔE_{SUR} was calculated from the following equation:

$$\Delta E_{SUR} = \alpha \text{ x } SASA + \beta, \quad (2)$$

where SASA was calculated using LCPO method [66], regression coefficient α was set to 0.005 and the regression offset β was set to 0.

3. Results and discussion

3.1. Modulation of $A\beta_{1-42}$ aggregation

Toxicity of Aβ and related Alzheimer's disease-associated neuronal loss have been clinically associated with the accumulation of oligomeric forms of the peptide which generally are known to precede amyloid fibril formation [72,73]. In vitro assays have shown that short incubation times, of 1.5–6 h, result in the formation of ThT positive oligomeric $A\beta_{1-42}$ assemblies that significantly associate with apoptotic neurons and cognitive dysfunction in a mouse model [74]. To obtain preliminary insights into the ability of isoquinoline alkaloids to modulate the accumulation of $A\beta_{1-42}$ oligomers we evaluated herein thioflavin (ThT) fluorescence intensity after 2 h incubation [75]. First of all, the $A\beta_{1-42}$ monomer (25 μM) was incubated with SA, CH or CO (25 μM). The extent of ThT-positive aggregation of $A\beta_{1-42}$ within this incubation time was then assessed by recording the fluorescence emission of ThT (12 μM, $\lambda_{ex} = 450$ nm, $\lambda_{em} = 485$ nm) (Fig. 2).

Data show that SA and CH reduce the ThT fluorescence signal by ~40% compared with $A\beta_{1-42}$ in the absence of these compounds. On the other hand, the berberine-like CO increased the aggregation level of $A\beta_{1-42}$ as indicated by a strong two-fold increase in ThT fluorescence intensity compared to untreated $A\beta_{1-42}$. These results show that berberine-like and benzo[*c*]phenanthridine alkaloids differently modulate $A\beta_{1-42}$ aggregation.

3.2. $A\beta_{1-42}$ conformational response to isoquinoline alkaloids

To investigate if the observed effects of isoquinoline alkaloids on $A\beta_{1-42}$ aggregation were accompanied by conformational variations, we performed circular dichroism (CD) time-dependent studies. The aggregation of $A\beta_{1-42}$, which reportedly coincides with increasing β-sheet content [76], was monitored using CD at different time points of incubation (0.5, 24 and 48 h, in PBS at 37 °C; Fig. 3). The obtained time-dependent CD profiles of $A\beta_{1-42}$ showed spectral changes in agreement with those reported in literature [11,77] with a progressive transition towards a β-sheet conformation at 24 h indicated by a broad band centered at ~225 nm, that is a spectral element previously assigned to this secondary structure in many amyloid systems [78–83].

At longer incubation times CD intensity at 225 nm showed a tendency to decrease (Fig. 3) suggestive of amyloid aggregation/precipitation as previously observed under similar conditions [77]. In parallel,

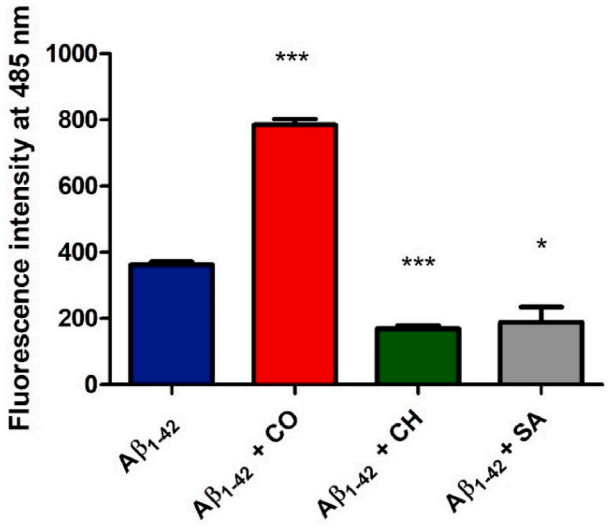

Fig. 2. SA and CH inhibit ThT-positive oligomer formation of $A\beta_{1-42}$, whereas CO induces ThT-positive assemblies. Solutions containing $A\beta_{1-42}$ at a concentration of 25 μM were incubated in the presence and absence of **SA, CH and CO (at 1:1 ratio)** at 37 °C for 2 h. ThT-positive aggregate formation was detected using ThT fluorescence intensity measurements at a fluorescence emission wavelength of 485 nm upon excitation at 450 nm. The reported values represent the results obtained from three independent experiments. The statistical significance of the replicates was assessed by p-values using paired two-tailed t-tests (GraphPad Prism).
*$p < 0.05$, **$p < 0.01$, and ***$p < 0.001$ compared with the control ('$A\beta_{1-42}$').

$A\beta_{1-42}$ was incubated, under the same experimental conditions, with the isoquinoline alkaloids (which did not contribute to the observed CD signal).

Remarkably, the presence of CO, already at t = 0.5 h of analysis, (Fig. 3) favors a β-like structure as indicated by a minimum at ~225 nm that, in the following 24 h, slightly shifts toward higher wavelengths (Fig. 3). The observed increase of Cotton effect for $A\beta_{1-42}$ in the presence of CO at 24 h (Fig. 3) can be ascribed to a stabilization of these secondary structures [84–89]. When comparing the CD spectra of $A\beta_{1-42}$ in the presence of all three compounds after 24 h, it became apparent that the presence of the three isoquinoline alkaloids induced differences in the structural organization of $A\beta_{1-42}$ (Fig. 3). The observed changes, impacting on both intensity and shape of spectra, were already described by Guo et al. [80], suggesting that benzo[*c*]phenanthridines partly limited β-sheet content of $A\beta_{1-42}$ leading to new structural elements. The effect is more appreciable for CH while the main significant variations are evident in the 210–220 nm range for SA.

3.3. Isoquinoline alkaloids interact with $A\beta_{1-42}$

To further evaluate the ability of isoquinoline alkaloids to interact with $A\beta_{1-42}$ we carried out SPR assays [90]. Binding profiles for all three molecules (Fig. 4) suggested the formation of complexes, in a concentration-dependent manner. Freshly dissolved $A\beta_{1-42}$, after HFIP treatment, was covalently immobilized on Sensor chip [91]. Kinetic parameters, reported in Table 1, allowed the estimation of thermodynamic dissociation constant values that appear in the low, for CO, high, for SA, and very high, for CH, micromolar range. The higher affinity exhibited by CO compared to CH and SA can be due to the faster association phase. Our data are in agreement with a previous study [91] that showed the ability of berberine-like inhibitors of $A\beta_{1-42}$ to interact with the polypeptide at low micromolar K_D values [91].

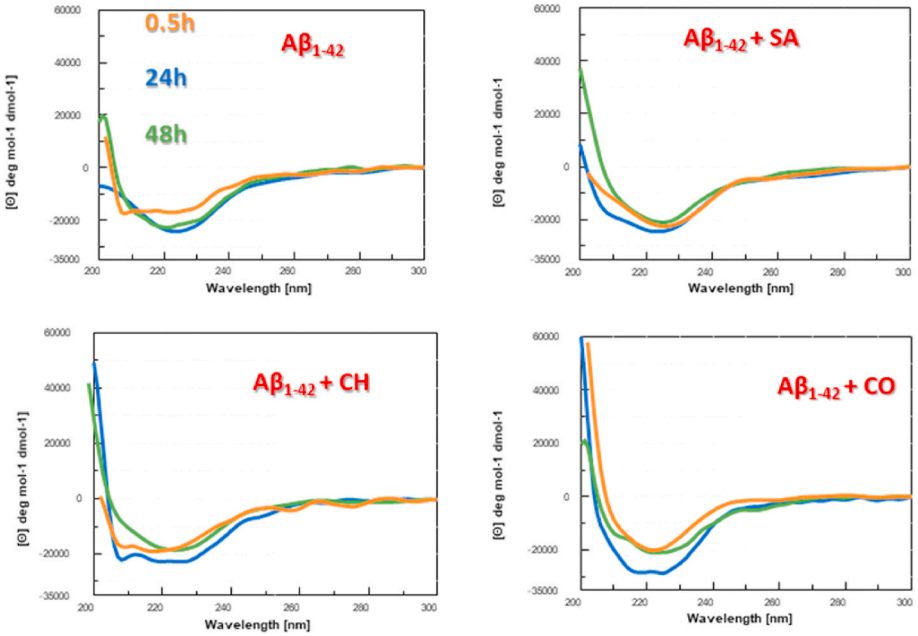

Fig. 3. Conformational response of Aβ$_{1-42}$ peptide to SA, CH and CO. Circular dichroism spectra of Aβ$_{1-42}$ (5 μM concentration in PBS, black line) and Aβ$_{1-42}$ in the presence of isoquinoline alkaloids (1:2 M ratio, peptide: small molecule) after 0.5 (orange), 24 (blue), and 48 (green) h of incubation at 37 °C.

3.4. Computational study of the interaction of SA, CH and CO with monomeric and fibrillar Aβ$_{1-42}$

To further explore the molecular-level interactions responsible for the observed modulating effects of Aβ$_{1-42}$ aggregation displayed by small molecules we performed *in silico* studies as described below.

3.5. Binding energies

3.5.1. Docking of ligands to monomers

The binding energies of the three ligands were estimated by means of Molecular Docking. Since Aβ peptides are intrinsically disordered, their native structures are transient and cannot be resolved experimentally.

Therefore, for our simulations we adopted three most representative Aβ$_{1-42}$ monomeric models obtained by clustering ensembles of monomeric Aβ$_{1-42}$ conformations at 300K from extensive all-atom Replica-Exchange and conventional MD simulations with explicit water model performed with various Amber and CHARMM force fields [54], as targets (Fig. 5). Because of the disordered character of monomeric Aβ$_{1-42}$ there is no possibility to treat properly flexibility of the receptor during docking procedure, therefore, we utilized three various Aβ$_{1-42}$ conformations to better sample the possible binding modes and which should minimize the impact of conformational selection. It should be noted that the use of multiple targets can significantly enhance the quality of docking results as shown by the McCammon group [92] and this approach is known as ensemble-based virtual screening.

As expected for similar small compounds, their modes of interactions appeared quite similar, but significant differences were observed in the number of possible binding modes (Table 2), which is higher for CO for all three monomeric structures. Conversely, the lowest number of binding modes was found for SA suggesting a more selective binding mechanism toward Aβ$_{1-42}$ with respect to the other compounds. The drug-amyloid interactions are stabilized by both hydrophobic and hydrogen bonds (three for SA and CH and one for CO, Fig. 6). Interestingly, CH and SA, contrary to CO, form hydrogen bonds with two histidine residue (His13 and His14), that are reported as responsible of the binding of ions, e.g. Cu^{2+}, which impacts Aβ$_{1-42}$ aggregation [93].

Averaging over all target structures in the best docking mode (mode 1) of the monomer, from Table 2 we obtain the binding energy $\Delta E_{bind} = -9.21$, -9.48 and -9.16 kcal/mol for CO, SA and CH, respectively

The highest interaction energy was observed for the least structured model 2, due to the disordered and extended character of this conformation allowing compounds to maximize the number of hydrogen bonds between molecules maintaining a high number of hydrophobic contacts (Table 3).

3.5.2. Docking of ligands to Aβ$_{1-42}$ tetramers

As oligomeric states are a bridging step between monomers and fibrils, we decided to study the impact of the three ligands on tetramers, that are considered crucial in Aβ$_{1-42}$ aggregation [94], by using models obtained in previous multi-scale MD simulations [66]. Similar to the monomeric Aβ$_{1-42}$, SA exhibited minor binding modes for all three tetrameric models (Table 4 and Fig. S1) confirming major selectivity of interaction. Averaging over three models of the tetramer and using data shown in Table 4, in the best docking mode we obtained $\Delta E_{bind} = -8.88$, -9.98, and -9.60 kcal/mol for CO, SA and CH, respectively. Which these values of the binding energy, IC50 of the three compounds is of order of μM. Moreover, the small differences in binding affinity of compounds to monomeric and tetrameric forms are probably due to compact forms of Aβ$_{1-42}$ tetramers, which did not allow many interactions with drugs even when more chains and possible binding sites are available. Overall, the high binding affinity of the studied compounds to oligomers indicates they can alter the fibril formation kinetics and pathways.

3.5.3. Docking of ligands to Aβ$_{1-42}$ protofibrils

The structure of Aβ$_{1-42}$ fibrils is still under debate. Old solid state NMR experiments showed that the monomer structure has the U-shape in the fibril state (here we call protofibril because we deal with a small number of chains) [95], but the S- and LS-shapes have been recently reported [96,97]. Assuming that protofibrils and fibrils have similar structures [98], we used the fibrillar structures deposited in PDB databank, for further docking simulation. Namely, we have chosen two experimental structures with U-shape (PDB ID 2LMN) [99] and LS-shape (PDB ID 2MXU) [96].

In both 2LMN and 2MXU models, the three ligands can bind in different regions depending on the docking mode (Figs. S2 and S3 in

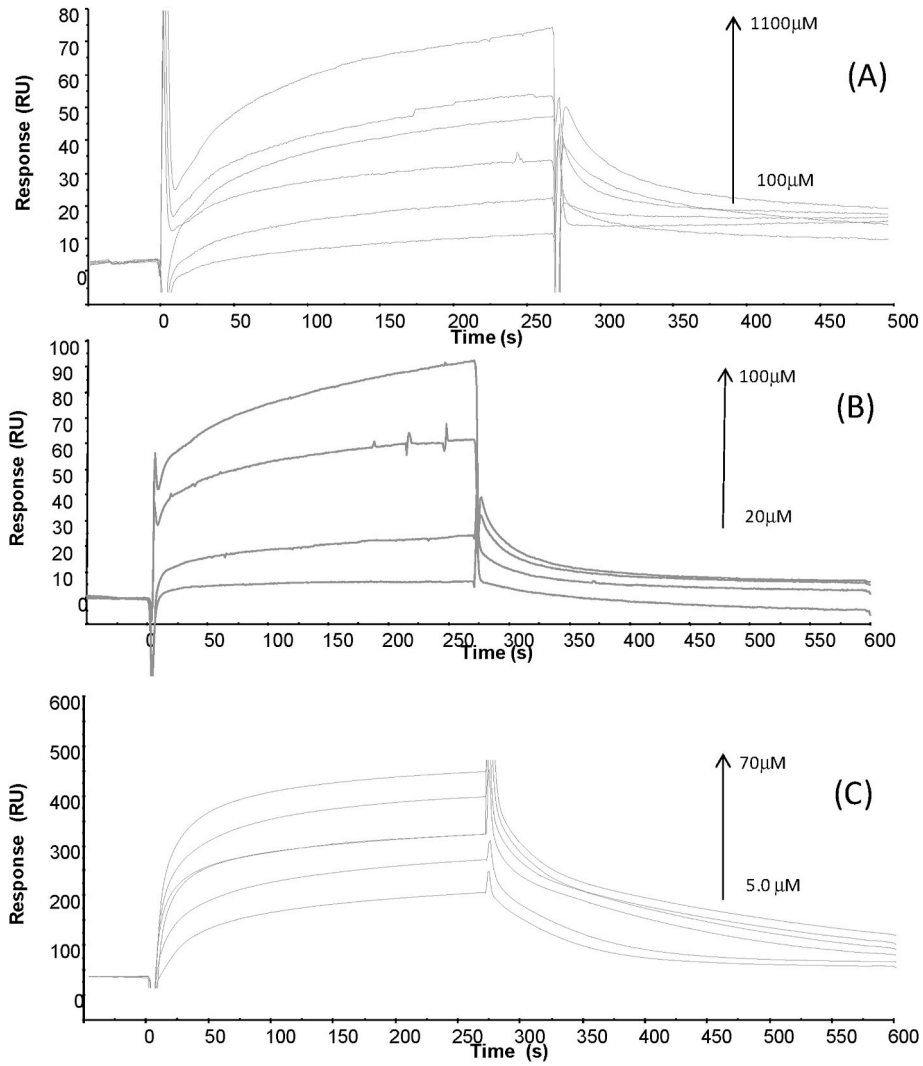

Fig. 4. Overlay of sensorgrams for the binding to immobilized $A\beta_{1\text{-}42}$ of (**A**) SA, (**B**) CH and (**C**) CO.

Table 1
SPR based equilibrium dissociation constants (K_D) and kinetic parameters for the interaction of $A\beta_{1\text{-}42}$ with SA, CH and CO using the BIA evaluation v.4.1 software. Data reported were obtained through SPR analyses using small molecules as analyte on immobilized $A\beta_{1\text{-}42}$.

	k_{on} ($M^{-1}s^{-1} \times 10^4$)	k_{off} ($s^{-1} \times 10^{-3}$)	K_D (μM)
Sanguinarine (SA)	13.1	6.07	463
Cheletrine (CH)	5.14	19.7	3.83*10 ^{3}
Coralyne (CO)	983	11.4	11.6

Supporting Information). In the docking mode with the lowest energy, they are all preferentially located in the loop region of 2LMN, while for 2MXU CO and CH seem to prefer the terminal part, while SA is mainly located in the middle of the structure. In analogy to the monomeric case, SA is endowed with the poorest variety in docking positions compared to the other two ligands (Figs. S2 and S3, and Table 5).

With the binding energy of about −12 kcal/mol (Table 5), IC50 of CO and SA with 2LMN and SA with 2MXU is in the range of nM. Overall, all ligands are more strongly associated with protofibrils than with monomers and tetramers. The identified potential for the ligands to interact with both monomeric, oligomeric and protofibrillar $A\beta_{1\text{-}42}$ suggests ample means for the ligands to modulate the subsequent aggregation process. Molecular Mechanics - Poisson Boltzmann Surface Area (MM-PBSA) docking assays on two compounds provided similar results (Figs. S4 and S5 and Table S1).

3.5.4. *Binding affinity of ligands to $A\beta_{1\text{-}42}$ protofibrils: MM-PBSA results*

Because in general docking results are not sufficiently reliable we performed molecular mechanics - Poisson Boltzmann surface area (MM-PBSA) assays on two compounds CO and SA. For each protofibril-ligand complex, the binding free energy was calculated for two binding sites obtained in modes 1 and 2 of the docking simulations. The details of simulations and the results are described in SI (Figs. S4 and S5 and Table S1), which show that, in agreement with the docking results, the ligands strongly bind to protofibrils with IC50 ~ nM.

3.5.5. *Molecular dynamics simulations*

In silico prediction of binding of the alkaloids to $A\beta_{1\text{-}42}$ indicated that the presence of a ligand can alter the rate of $A\beta_{1\text{-}42}$ aggregation, but it is unclear if it accelerates or slows down aggregation. On the other hand, our *in vitro* experiment demonstrated that CO speeds up fibril formation, while SA retards it. Thus, to clarify this issue, we performed MD simulations with 16 $A\beta_{1\text{-}42}$ chains in the absence or presence of CO and SA to mimic the first stages of $A\beta_{1\text{-}42}$ aggregation from semi-extended non-interacting chains. Studies of early aggregations stages of Aβ are believed to be key to understand the whole process and are commonly performed [100], even though the computational studies of it on all-atom level cannot reach equilibration, which would require probably minutes of real time [101].The simulation started from the initial

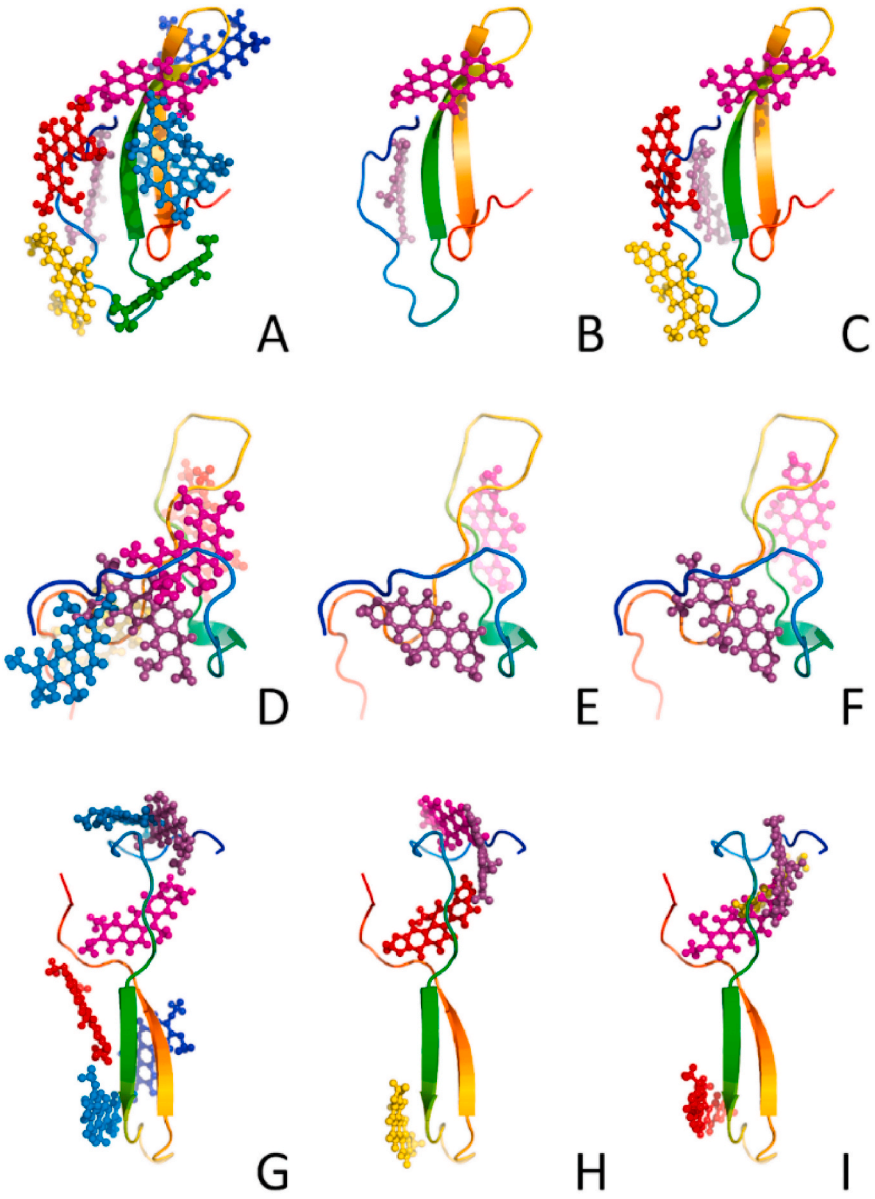

Fig. 5. Representations of docking positions of CO (left column: A, D, G), SA (middle column: B, E, H), and CH (right column: C, F, I) to three models of monomeric $A\beta_{1\text{-}42}$ (presented as rainbow-colored cartoons).

Table 2
AutoDock-predicted binding energies (kcal/mol) for the binding of the compounds CO, SA, and CH to three representative amyloid monomeric models obtained in the previous simulation study [50].

Binding Mode	$A\beta_{1\text{-}42}$ Model 1			$A\beta_{1\text{-}42}$ Model 2			$A\beta_{1\text{-}42}$ Model 3		
	CO	SA	CH	CO	SA	CH	CO	SA	CH
1	−8.03	−9.10	−8.59	−10.17	−10.26	−10.07	−9.44	−9.07	−8.82
2	−6.68	−7.24	−7.39	−7.53	−8.58	−8.36	−8.11	−8.99	−8.31
3	−6.36		−6.05	−7.52			−6.68	−8.69	−7.05
4	−6.24		−6.03	−7.07			−6.58	−6.87	−6.86
5	−5.57			−7.00			−5.84		
6	−5.42						−5.30		
7	−5.34								
8	−5.28								

configuration of the 16 non-interacting randomly generated $A\beta_{1\text{-}42}$ chains in the presence of ligands in a 1:1 ratio (Fig. 7). For each set, we carried out two trajectories of 800 ns: this short interval even if it does not allow reaching equilibrium provides insights the initial steps of the aggregation.

Simulations showed that the flexibility of the chains was unaffected by the presence of the ligands (Table 6), as RMSD, gyration radius Rg, solvent accessible surface area (SASA), and end-to-end (N–C) distance

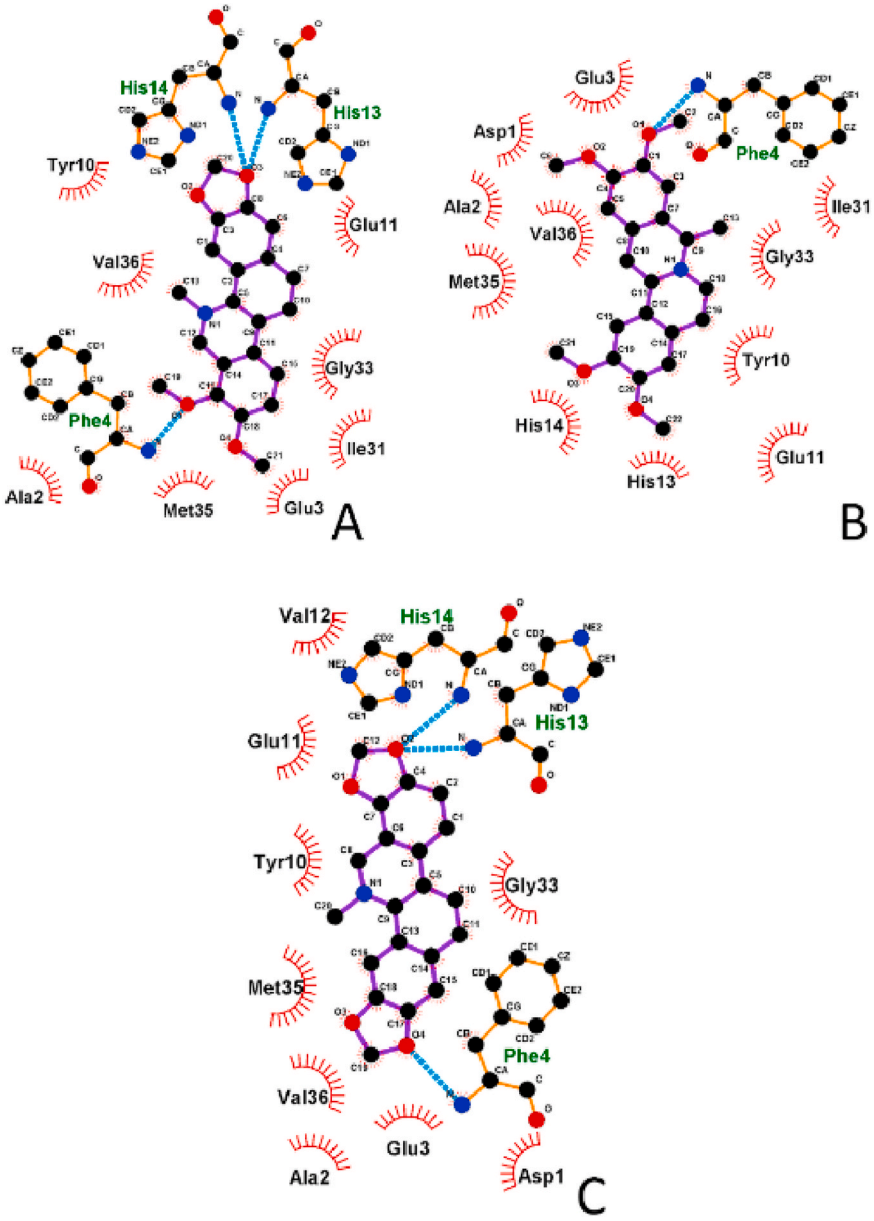

Fig. 6. Schematic representation of the strongest binding mode of monomeric $A\beta_{1\text{-}42}$ to compounds (monomeric model 2, binding mode 1; see Table 2 for more details) showed in 2D form for: A) CH, B) CO, C) SA. $A\beta_{1\text{-}42}$ residues involved in hydrophobic interactions with compounds are showed by red lines and black three-letter residue codes, hydrogen bonds are represented by cyan dashed lines and green three-letter residue codes. For clarity, hydrogens are not presented on the plot.

Table 3
Number of hydrogen bonds (HB) and hydrophobic interactions (HI) between monomeric $A\beta_{1\text{-}42}$ models and the ligands CO, SA, and CH in the strongest binding mode (mode 1).

	$A\beta_{1\text{-}42}$ Model 1		$A\beta_{1\text{-}42}$ Model 2		$A\beta_{1\text{-}42}$ Model 3	
	HI	*HB*	*HI*	*HB*	*HI*	*HB*
CO	*10*	*1*	*11*	*1*	*9*	*1*
SA	*10*	*1*	*9*	*3*	*7*	*1*
CH	*9*	*1*	*8*	*3*	*7*	*1*

did not vary significantly in absence or presence of the ligand. This was expected due to the semi-extended nature of the initial $A\beta_{1\text{-}42}$ chains, which in the early aggregation steps firstly try to hide hydrophobic residues from the solvent and only then form stable interactions with other chains forming oligomeric structures [102,103]. Decrease of the number of interchain contacts indicates that both compounds are interacting with $A\beta_{1\text{-}42}$ replacing some of the interaction which normally would form between chains. In general, calculated properties are quite dispersed, which is visible as high standard deviation values in Table 6, a feature caused by averaging over 16 chains, 2 trajectories and snapshots from the second halves of the simulations which are not fully equilibrated, and by the fact that $A\beta_{1\text{-}42}$ chains are subjected to large conformational changes. However, even relatively small changes at early aggregation steps caused e.g. by the presence of external compounds, can significantly impact aggregation pathways and fibrilization process [104,105]. It was also previously reported that the beta content of $A\beta_{1\text{-}42}$ monomers exponentially affects the aggregation rate [106], therefore we believe that these small changes may have significant impact on the behavior of the $A\beta_{1\text{-}42}$ taking into account its disordered nature in low-mass forms, which increase its susceptibility to external factors.

Both ligands reduced the population of monomers: a remarkable variation in the population of tetramers, heptamers, 14- and 15-mers

Table 4
AutoDock-predicted binding energies (kcal/mol) for the binding of the CO, SA, and CH to three representative amyloid tetrameric models obtained in the previous simulation study [62] (models 1, 2, and 3 correspond to tetramers 1, 3, and 5 from the mentioned work, respectively).

Binding Mode	$A\beta_{1-42}$ tetramer 1			$A\beta_{1-42}$ tetramer 2			$A\beta_{1-42}$ tetramer 3		
	CO	SA	CH	CO	SA	CH	CO	SA	CH
1	−9.06	−9.97	−9.72	−9.36	−9.52	−9.26	−8.21	−10.45	−9.81
2	−8.48	−9.89	−8.93	−8.84	−9.46	−9.05	−7.94	−8.44	−8.43
3	−7.56	−9.14	−8.78	−8.80	−9.13	−7.91	−7.24	−8.26	−8.32
4	−7.51		−7.19	−7.28	−8.34	−7.42	−7.02	−7.96	−7.57
5	−6.43		−7.13	−7.25	−7.52	−7.33	−7.00	−7.68	−7.50
6	−5.77		−6.55	−7.04		−6.96	−6.80		−6.88
7							−6.55		−6.50
8							−6.01		−6.48

Table 5
AutoDock-predicted binding energies (kcal/mol) of the clustered orientations with 2LMN and 2MXU fibril models.

Mode	2LMN			2MXU			
	CO	SA	CH	CO	SA	CH	Color
1	−12.12	−12.16	−10.93	−10.41	−11.76	−10.89	Purple
2	−11.90	−10.71	−10.83	−9.70	−10.92	−10.36	Magenta
3	−10.07	−10.50	−9.83	−8.71	−10.09	−9.73	Red
4	−10.00	−10.37	−9.71	−7.14	−9.98	−7.96	Yellow
5	−9.97	−9.94	−9.60	−6.34		−7.87	Cyan
6	−8.84		−9.56			−7.80	Teal
7	−8.78		−9.42				Blue
8	−8.37		−8.15				Green
9	−6.72		−6.95				Darkgrey
10	−6.21						Lightgrey

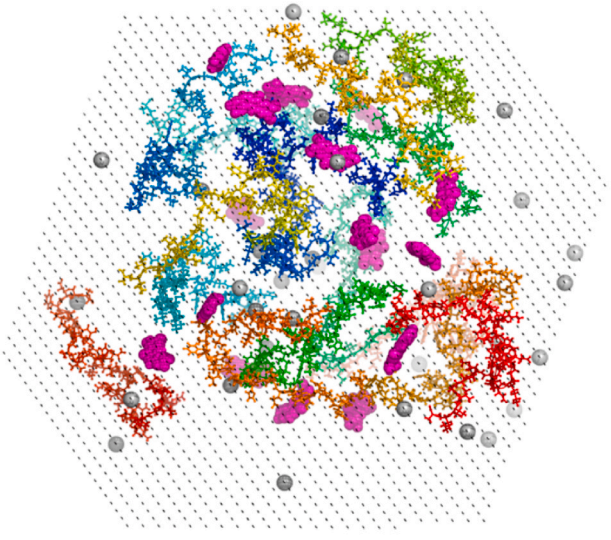

Fig. 7. Initial structure of the 16 $A\beta_{1-42}$ chains with SA in 1:1 ratio. $A\beta_{1-42}$ is represented by ball-and-sticks, SA by magenta spheres, counter ions by light-grey sphere, water by black dots.

Table 6
Calculated average properties of the $A\beta_{1-42}$chains from simulations of 16 chains with standard deviations. Other details are given in Fig. S6.

	$A\beta_{1-42}$	$A\beta_{1-42}$+ CO	$A\beta_{1-42}$+ SA
RMSD [Å]	10.97 ± 0.49	11.30 ± 0.36	11.52 ± 0.40
Rg [Å]	14.04 ± 0.28	14.45 ± 0.63	14.21 ± 0.41
SASA [nm^2]	553.4 ± 21.1	576.6 ± 24.2	569.0 ± 20.3
N–C distance [Å]	33.64 ± 1.98	32.40 ± 2.29	34.24 ± 1.29
Number of contacts between chains	3.76 ± 0.25	3.06 ± 0.33	3.02 ± 0.19
Alpha content [%]	3.12 ± 1.11	2.92 ± 1.83	3.72 ± 0.50
Beta content [%]	4.04 ± 0.72	5.01 ± 0.81	2.33 ± 0.66

(Fig. S7) was observed, which means that aggregation pathways to the fibril state are extensively modified by the ligands. In addition to size of the oligomers, our data confirm the secondary content is the prevalent factor governing aggregation rate of $A\beta_{1-42}$ [107], suggesting that it could be in relation with the opposite effects by the SA and CO on the aggregation.

4. Conclusion

Herein we studied early $A\beta_{1-42}$ aggregation stages in the presence of three alkaloids and our preliminary findings suggested that aromatic tetracycles with benzo[*c*]phenanthridine and berberine nuclei and similar functionalization of the aromatic core may oppositely affect the aggregation of $A\beta_{1-42}$ peptide.

While benzo[*c*]phenanthridines SA and CH seemed to inhibit aggregation, the berberine-like CO increased propensity for $A\beta_{1-42}$ to aggregate, showing also the highest affinity for monomeric $A\beta_{1-42}$, as revealed by SPR experiments, and it displayed the highest variety of binding modes (as found *in silico*). These observations suggest that, different from benzo[*c*]phenanthridines, the bent berberine-like structure of CO can be accommodated in a higher number of diverse $A\beta_{1-42}$ conformations. The presence of CO also led to increased $A\beta_{1-42}$ β-content as revealed by CD experiments and MD calculations: this effect appears in perfect agreement with the promotion of $A\beta_{1-42}$ aggregation observed in the ThT assay. Both docking and MM-PBSA simulations showed that all three studied alkaloids interact with monomeric, oligomeric and protofibrillar $A\beta_{1-42}$. Our *in silico* study revealed that SA inhibits the assembly of $A\beta_{1-42}$ into aggregates as a result of helix stabilization in the $A\beta_{1-42}$ amyloid structure. On the contrary, the aggregation promoting effect caused by CO possibly occurs through enhancement of the β structures, which are predominantly reported in the fibril state. Interestingly, both benzo[*c*]phenanthridine and berberine derivatives are able to modulate the amyloid aggregation pathways by showing differences in the population of different oligomeric states, and in particular the $A\beta_{1-42}$ oligomer assembly state undergoes significant changes upon ligand binding.

Finally, since berberine and Ber-D (Fig. S8), compounds differing from CO by carrying one non-aromatic ring (berberine) or free hydroxyl-groups besides the non-aromatic ring (Ber-D), both inhibit $A\beta_{1-42}$ aggregation [22], future synthetic efforts and, biological studies should be carried out on chelerythrine-derived compounds CH-D1 and CH-D2 (Fig. S8) as promising candidates as neurodrugs in the family of the benzo[*c*]phenanthridine alkaloids [22].

Funding

We are grateful to the financial support received from Campania Region, Italy [POR-FESR 2014–2020 project PON03PE_0060_4], "Combattere la resistenza tumorale: piattaforma integrata multi-disciplinare per un approccio tecnologico innovativo alle oncoterapie-Campania Oncoterapie" (Project N. B61G18000470007) and ZonMw for Memorabel project "Exploring the potential of multi-target treatment for Alzheimer's disease" (Project N. 733050304). Mai Suan Li was supported by Department of Science and Technology, Ho Chi Minh city, Vietnam (grant No. 07/2019/HĐ-KHCNTT) and Narodowe Centrum Nauki (NCN) in Poland (grant No 2019/35/B/ST4/02086).

CRediT authorship contribution statement

Daniela Marasco: Conceptualization, Investigation, Data curation, Writing - original draft. **Caterina Vicidomini:** Investigation, Methodology, Data curation, Validation. **Pawel Krupa:** Investigation, Methodology, Data curation, Writing - original draft, Writing - review & editing. **Federica Cioffi:** Investigation, Methodology. **Pham Dinh Quoc Huy:** Investigation, Methodology. **Mai Suan Li:** Investigation, Methodology, Writing - original draft. **Daniele Florio:** Investigation, Methodology. **Kerensa Broersen:** Investigation, Methodology, Writing - original draft. **Maria Francesca De Pandis:** Conceptualization, Writing - original draft. **Giovanni N. Roviello:** Supervision, Conceptualization, Investigation, Methodology, Data curation, Writing - original draft.

Declaration of competing interest

The authors declare that they have no known competing financial interests or personal relationships that could have appeared to influence the work reported in this paper.

Appendix A. Supplementary data

Supplementary data to this article can be found online at https://doi.org/10.1016/j.cbi.2020.109300.

References

[1] J.-C. Rochet, P.T. Lansbury, Amyloid fibrillogenesis: themes and variations, Curr. Opin. Struct. Biol. 10 (2000) 60–68.
[2] J. Nasica-Labouze, P.H. Nguyen, F. Sterpone, O. Berthoumieu, N.-V. Buchete, S. Coté, A. De Simone, A.J. Doig, P. Faller, A. Garcia, A. Laio, M.S. Li, S. Melchionna, N. Mousseau, Y. Mu, A. Paravastu, S. Pasquali, D.J. Rosenman, B. Strodel, B. Tarus, J.H. Viles, T. Zhang, C. Wang, P. Derreumaux, Amyloid β protein and Alzheimer's disease: when computer simulations complement experimental studies, Chem. Rev. 115 (2015) 3518–3563.
[3] J. Weller, A. Budson, Current understanding of Alzheimer's disease diagnosis and treatment, F1000Research 7 (2018) 1161.
[4] K. Blennow, M.J. de Leon, H. Zetterberg, Alzheimer's disease, Lancet 368 (2006) 387–403.
[5] L. Gu, Z. Guo, Alzheimer's Aβ42 and Aβ40 peptides form interlaced amyloid fibrils, J. Neurochem. 126 (2013) 305–311.
[6] Z. van Helmond, J.S. Miners, P.G. Kehoe, S. Love, Oligomeric Aβ in alzheimer's disease: relationship to plaque and tangle Pathology,APOEGenotype and cerebral amyloid angiopathy, Brain Pathol. 20 (2010) 468–480.
[7] A. Jan, O. Adolfsson, I. Allaman, A.-L. Buccarello, P.J. Magistretti, A. Pfeifer, A. Muhs, H.A. Lashuel, Aβ42 neurotoxicity is mediated by ongoing nucleated polymerization process rather than by discrete Aβ42 species, J. Biol. Chem. 286 (2011) 8585–8596.
[8] K.H. Gylys, J.A. Fein, F. Yang, C.A. Miller, G.M. Cole, Increased cholesterol in Aβ-positive nerve terminals from Alzheimer's disease cortex, Neurobiol. Aging 28 (2007) 8–17.
[9] A.J. Doig, P. Derreumaux, Inhibition of protein aggregation and amyloid formation by small molecules, Curr. Opin. Struct. Biol. 30 (2015) 50–56.
[10] F. Re, C. Airoldi, C. Zona, M. Masserini, B.L. Ferla, N. Quattrocchi, F. Nicotra, Beta amyloid aggregation inhibitors: small molecules as candidate drugs for therapy of alzheimers disease, Curr. Med. Chem. 17 (2010) 2990–3006.
[11] C. Vicidomini, F. Cioffi, K. Broersen, V. Roviello, C. Riccardi, D. Montesarchio, D. Capasso, S.D. Gaetano, D. Musumeci, G.N. Roviello, Benzodifurans for biomedical applications: BZ4, a selective anti-proliferative and anti-amyloid lead compound, Future Med. Chem. 11 (2019) 285–302.
[12] Y. Wang, D.C. Latshaw, C.K. Hall, Aggregation of aβ(17–36) in the presence of naturally occurring phenolic inhibitors using coarse-grained simulations, J. Mol. Biol. 429 (2017) 3893–3908.
[13] E.A. Permyakov, M.H. Viet, C.-Y. Chen, C.-K. Hu, Y.-R. Chen, M.S. Li, Discovery of dihydrochalcone as potential lead for Alzheimer's disease: in silico and in vitro study, PloS One 8 (2013), e79151.
[14] S.T. Ngo, M.S. Li, Curcumin binds to aβ1–40 peptides and fibrils stronger than ibuprofen and naproxen, J. Phys. Chem. B 116 (2012) 10165–10175.
[15] K.W. Bentley, The Isoquinoline Alkaloids, 1975, pp. 259–348.
[16] I. Orhan, B. Özçelik, T. Karaoğlu, B. Şener, Antiviral and antimicrobial profiles of selected isoquinoline alkaloids from fumaria and corydalis species, Z. Naturforsch. C Biosci. 62 (2007) 19–26.
[17] S. Mehrzadi, I. Fatemi, M. Esmaeilizadeh, H. Ghaznavi, H. Kalantar, M. Goudarzi, Hepatoprotective effect of berberine against methotrexate induced liver toxicity in rats, Biomed. Pharmacother. 97 (2018) 233–239.
[18] O.J. Patiño Ladino, L.E. Cuca Suárez, Isoquinoline alkaloids of Zanthoxylum quinduense (Rutaceae), Biochem. Systemat. Ecol. 38 (2010) 853–856.
[19] M.I.A. Kim, K.-H. Cho, M.-S. Shin, J.-M. Lee, H.-S. Cho, C.-J. Kim, D.-H. Shin, H. J. Yang, Berberine prevents nigrostriatal dopaminergic neuronal loss and suppresses hippocampal apoptosis in mice with Parkinson's disease, Int. J. Mol. Med. 33 (2014) 870–878.
[20] T. Ahmed, A.-u.-H. Gilani, M. Abdollahi, M. Daglia, S.F. Nabavi, S.M. Nabavi, Berberine and neurodegeneration: a review of literature, Pharmacol. Rep. 67 (2015) 970–979.
[21] K.S. Shin, H.S. Choi, T.T. Zhao, K.H. Suh, I.H. Kwon, S.O. Choi, M.K. Lee, Neurotoxic effects of berberine on long-term l-DOPA administration in 6-hydroxydopamine-lesioned rat model of Parkinson's disease, Arch Pharm. Res. (Seoul) 36 (2013) 759–767.
[22] K. Rajasekhar, S. Samanta, V. Bagoband, N.A. Murugan, T. Govindaraju, Antioxidant berberine-derivative inhibits multifaceted amyloid toxicity, iScience 23 (2020) 101005.
[23] K.-Y. Zee-Cheng, K.D. Paull, C.C. Cheng, Experimental antileukemic agents. Coralyne, analogs, and related compounds, J. Med. Chem. 17 (1974) 347–351.
[24] F. Xing, G. Song, J. Ren, J.B. Chaires, X. Qu, Molecular recognition of nucleic acids: coralyne binds strongly to poly(A), FEBS (Fed. Eur. Biochem. Soc.) Lett. 579 (2005) 5035–5039.
[25] G. Pi, P. Ren, J. Yu, R. Shi, Z. Yuan, C. Wang, Separation of sanguinarine and chelerythrine in Macleaya cordata (Willd) R. Br. based on methyl acrylate-co-divinylbenzene macroporous adsorbents, J. Chromatogr. A 1192 (2008) 17–24.
[26] J. Dostál, M. Potáček, Quaternary benzo[c]phenanthridine alkaloids, Collect. Czech Chem. Commun. 55 (1990) 2840–2873.
[27] R. Zhang, X.W. Wang, J.Y. Zhu, L.L. Liu, Y.C. Liu, H. Zhu, Dietary sanguinarine affected immune response, digestive enzyme activity and intestinal microbiota of Koi carp (cryprinus carpiod), Aquaculture 502 (2019) 72–79.
[28] C.M. Uhlar, A.S. Whitehead, Serum amyloid A, the major vertebrate acute-phase reactant, Eur. J. Biochem. 265 (1999) 501–523.
[29] T. Miida, T. Yamada, U. Seino, M. Ito, Y. Fueki, A. Takahashi, K. Kosuge, S. Soda, O. Hanyu, K. Obayashi, O. Miyazaki, M. Okada, Serum amyloid A (SAA)-induced remodeling of CSF-HDL, Biochim. Biophys. Acta Mol. Cell Biol. Lipids 1761 (2006) 424–433.
[30] H. Li, X. Xiang, H. Ren, L. Xu, L. Zhao, X. Chen, H. Long, Q. Wang, Q. Wu, Serum Amyloid A is a biomarker of severe Coronavirus Disease and poor prognosis, J. Infect. 80 (6) (2020 Jun) 646–655, https://doi.org/10.1016/j.jinf.2020.03.035.
[31] T. Wang, Z. Du, F. Zhu, Z. Cao, Y. An, Y. Gao, B. Jiang, Comorbidities and multi-organ injuries in the treatment of COVID-19, Lancet 395 (2020) e52.
[32] H.A. Rothan, S.N. Byrareddy, The epidemiology and pathogenesis of coronavirus disease (COVID-19) outbreak, J. Autoimmun. 109 (2020) 102433.
[33] M. Costanzo, M.A.R. De Giglio, G.N. Roviello, SARS CoV-2: recent reports on antiviral therapies based on lopinavir/ritonavir, darunavir/umifenovir, hydroxychloroquine, remdesivir, favipiravir and other drugs for the treatment of the new coronavirus, Curr. Med. Chem. 27 (2020).
[34] V. Roviello, G.N. Roviello, Lower COVID-19 mortality in Italian forested areas suggests immunoprotection by Mediterranean plants, Environ. Chem. Lett. (2020 Aug 14) 1–12, https://doi.org/10.1007/s10311-020-01063-0.
[35] C. Wiart, Lead Compounds from Medicinal Plants for the Treatment of Neurodegenerative Diseases, Academic Press, London, 2014.
[36] G. Brunhofer, A. Fallarero, D. Karlsson, A. Batista-Gonzalez, P. Shinde, C. Gopi Mohan, P. Vuorela, Exploration of natural compounds as sources of new bifunctional scaffolds targeting cholinesterases and beta amyloid aggregation: the case of chelerythrine, Bioorg. Med. Chem. 20 (2012) 6669–6679.
[37] S.T. Ngo, M.S. Li, Top-leads from natural products for treatment of Alzheimer's disease: docking and molecular dynamics study, Mol. Simulat. 39 (2013) 279–291.

[38] K. Broersen, W. Jonckheere, J. Rozenski, A. Vandersteen, K. Pauwels, A. Pastore, F. Rousseau, J. Schymkowitz, A standardized and biocompatible preparation of aggregate-free amyloid beta peptide for biophysical and biological studies of Alzheimer's disease, Protein Eng. Des. Sel. 24 (2011) 743–750.
[39] M. Moccia, G.N. Roviello, E.M. Bucci, C. Pedone, M. Saviano, Synthesis of a l-lysine-based alternate alpha,epsilon-peptide: a novel linear polycation with nucleic acids-binding ability, Int. J. Pharm. 397 (2010) 179–183.
[40] G.N. Roviello, S.D. Gaetano, D. Capasso, A. Cesarani, E.M. Bucci, C. Pedone, Synthesis, spectroscopic studies and biological activity of a novel nucleopeptide with Moloney murine leukemia virus reverse transcriptase inhibitory activity, Amino Acids 38 (2010) 1489–1496.
[41] G.N. Roviello, V. Roviello, I. Autiero, M. Saviano, Solid phase synthesis of TyrT, a thymine–tyrosine conjugate with poly(A) RNA-binding ability, RSC Adv. 6 (2016) 27607–27613.
[42] G.N. Roviello, C. Crescenzo, D. Capasso, S. Di Gaetano, S. Franco, E.M. Bucci, C. Pedone, Synthesis of a novel Fmoc-protected nucleoaminoacid for the solid phase assembly of 4-piperidyl glycine/l-arginine-containing nucleopeptides and preliminary RNA interaction studies, Amino Acids 39 (2010) 795–800.
[43] G.N. Roviello, Novel insights into nucleoamino acids: biomolecular recognition and aggregation studies of a thymine-conjugated l-phenyl alanine, Amino Acids 50 (2018) 933–941.
[44] M.A. Fik-Jaskółka, A.F. Mkrtchyan, A.S. Saghyan, R. Palumbo, A. Belter, L. A. Hayriyan, H. Simonyan, V. Roviello, G.N. Roviello, Spectroscopic and SEM evidences for G4-DNA binding by a synthetic alkyne-containing amino acid with anticancer activity, Spectrochim. Acta Mol. Biomol. Spectrosc. 229 (2020) 117884.
[45] D. Musumeci, A. Mokhir, G.N. Roviello, Synthesis and nucleic acid binding evaluation of a thyminyl L-diaminobutanoic acid-based nucleopeptide, Bioorg. Chem. (2020) 103862.
[46] G. Oliviero, N. Borbone, J. Amato, S. D'Errico, A. Galeone, G. Piccialli, M. Varra, L. Mayol, Synthesis of quadruplex-forming tetra-end-linked oligonucleotides: effects of the linker size on quadruplex topology and stability, Biopolymers 91 (2009) 466–477.
[47] A.S. Saghyan, H.M. Simonyan, S.G. Petrosyan, A.V. Geolchanyan, G.N. Roviello, D. Musumeci, V. Roviello, Thiophenyl-substituted triazolyl-thione l-alanine: asymmetric synthesis, aggregation and biological properties, Amino Acids 46 (2014) 2325–2332.
[48] G.N. Roviello, M. Moccia, R. Sapio, M. Valente, E.M. Bucci, M. Castiglione, C. Pedone, G. Perretta, E. Benedetti, D. Musumeci, Synthesis, characterization and hybridization studies of new nucleo-gamma-peptides based on diaminobutyric acid, J. Pept. Sci. 12 (2006) 829–835.
[49] A. Carella, V. Roviello, R. Iannitti, R. Palumbo, S. La Manna, D. Marasco, M. Trifuoggi, R. Diana, G.N. Roviello, Evaluating the biological properties of synthetic 4-nitrophenyl functionalized benzofuran derivatives with telomeric DNA binding and antiproliferative activities, Int. J. Biol. Macromol. 121 (2019) 77–88.
[50] D. Musumeci, G.N. Roviello, G. Rigione, D. Capasso, S. Di Gaetano, C. Riccardi, V. Roviello, D. Montesarchio, Benzodifuran derivatives as potential antiproliferative agents: Possible correlation between their bioactivity and aggregation properties, Chempluschem 82 (2) (2017 Feb) 251–260, https://doi.org/10.1002/cplu.201600547.
[51] V. D'Atri, G. Oliviero, J. Amato, N. Borbone, S. D'Errico, L. Mayol, V. Piccialli, S. Haider, B. Hoorelbeke, J. Balzarini, G. Piccialli, New anti-HIV aptamers based on tetra-end-linked DNA G-quadruplexes: effect of the base sequence on anti-HIV activity, Chem Commun (Camb) 48 (76) (2012 Oct 4) 9516–9518, https://doi.org/10.1039/c2cc34399a.
[52] G.N. Roviello, D. Musumeci, M. Castiglione, E.M. Bucci, C. Pedone, E. Benedetti, Solid phase synthesis and RNA-binding studies of a serum-resistant nucleo-ε-peptide, J. Pept. Scie. Off. Publ. Eur. Pept. Soc. 15 (3) (2009) 155–160.
[53] G.N. Roviello, G. Roviello, D. Musumeci, E.M. Bucci, C. Pedone, Dakin–West reaction on 1-thyminyl acetic acid for the synthesis of 1, 3-bis (1-thyminyl)-2-propanone, a heteroaromatic compound with nucleopeptide-binding properties, Amino Acids 43 (4) (2012) 1615–1623.
[54] P. Krupa, P.D. Quoc Huy, M.S. Li, Properties of monomeric Aβ42 probed by different sampling methods and force fields: role of energy components, J. Chem. Phys. 151 (2019), 055101.
[55] M.J. Frisch, G.W. Trucks, H.B. Schlegel, G.E. Scuseria, M.A. Robb, J. R. Cheeseman, G. Scalmani, V. Barone, G.A. Petersson, H. Nakatsuji, X. Li, M. Caricato, A.V. Marenich, J. Bloino, B.G. Janesko, R. Gomperts, B. Mennucci, H. P. Hratchian, J.V. Ortiz, A.F. Izmaylov, J.L. Sonnenberg, Williams, F. Ding, F. Lipparini, F. Egidi, J. Goings, B. Peng, A. Petrone, T. Henderson, D. Ranasinghe, V.G. Zakrzewski, J. Gao, N. Rega, G. Zheng, W. Liang, M. Hada, M. Ehara, K. Toyota, R. Fukuda, J. Hasegawa, M. Ishida, T. Nakajima, Y. Honda, O. Kitao, H. Nakai, T. Vreven, K. Throssell, J.A. Montgomery Jr., J.E. Peralta, F. Ogliaro, M. J. Bearpark, J.J. Heyd, E.N. Brothers, K.N. Kudin, V.N. Staroverov, T.A. Keith, R. Kobayashi, J. Normand, K. Raghavachari, A.P. Rendell, J.C. Burant, S. S. Iyengar, J. Tomasi, M. Cossi, J.M. Millam, M. Klene, C. Adamo, R. Cammi, J. W. Ochterski, R.L. Martin, K. Morokuma, O. Farkas, J.B. Foresman, D.J. Fox, Gaussian 16, Rev. C.01, Wallingford, CT, 2016.
[56] A. Jakalian, D.B. Jack, C.I. Bayly, Fast, efficient generation of high-quality atomic charges. AM1-BCC model: II. Parameterization and validation, J. Comput. Chem. 23 (2002) 1623–1641.
[57] J. Wang, R.M. Wolf, J.W. Caldwell, P.A. Kollman, D.A. Case, Development and testing of a general amber force field, J. Comput. Chem. 25 (2004) 1157–1174.
[58] G.M. Morris, R. Huey, W. Lindstrom, M.F. Sanner, R.K. Belew, D.S. Goodsell, A. J. Olson, AutoDock4 and AutoDockTools4: automated docking with selective receptor flexibility, J. Comput. Chem. 30 (2009) 2785–2791.
[59] N.T. Nguyen, T.H. Nguyen, T.N.H. Pham, N.T. Huy, M.V. Bay, M.Q. Pham, P. C. Nam, V.V. Vu, S.T. Ngo, Autodock Vina adopts more accurate binding poses but Autodock4 forms better binding affinity, J. Chem. Inf. Model. 60 (2019) 204–211.
[60] A. Castro-Alvarez, A.M. Costa, J. Vilarrasa, The performance of several docking programs at reproducing protein-macrolide-like crystal structures, Molecules (2017) 22.
[61] L. Ferreira, R. dos Santos, G. Oliva, A. Andricopulo, Molecular docking and structure-based drug design strategies, Molecules 20 (2015) 13384–13421.
[62] K.P.S. Adinarayana, R.K. Devi, Protein-Ligand interaction studies on 2, 4, 6-trisubstituted triazine derivatives as anti-malarial DHFR agents using AutoDock, Bioinformation 6 (2011) 74–77.
[63] J.A. Maier, C. Martinez, K. Kasavajhala, L. Wickstrom, K.E. Hauser, C. Simmerling, ff14SB: improving the accuracy of protein side chain and backbone parameters from ff99SB, J. Chem. Theor. Comput. 11 (2015) 3696–3713.
[64] W.L. Jorgensen, J. Chandrasekhar, J.D. Madura, R.W. Impey, M.L. Klein, Comparison of simple potential functions for simulating liquid water, J. Chem. Phys. 79 (1983) 926–935.
[65] B. Barz, Q. Liao, B. Strodel, Pathways of amyloid-β aggregation depend on oligomer shape, J. Am. Chem. Soc. 140 (2017) 319–327.
[66] H.L. Nguyen, P. Krupa, N.M. Hai, H.Q. Linh, M.S. Li, Structure and physicochemical properties of the Aβ42 tetramer: multiscale molecular dynamics simulations, J. Phys. Chem. B 123 (2019) 7253–7269.
[67] Ł. Mioduszewski, M. Cieplak, Protein droplets in systems of disordered homopeptides and the amyloid glass phase, Phys. Chem. Chem. Phys. 22 (2020) 15592–15599.
[68] C. Tian, K. Kasavajhala, K.A.A. Belfon, L. Raguette, H. Huang, A.N. Migues, J. Bickel, Y. Wang, J. Pincay, Q. Wu, C. Simmerling, ff19SB: amino-acid-specific protein backbone parameters trained against quantum mechanics energy surfaces in solution, J. Chem. Theor. Comput. 16 (2019) 528–552.
[69] S. Izadi, R. Anandakrishnan, A.V. Onufriev, Building water models: a different approach, J. Phys. Chem. Lett. 5 (2014) 3863–3871.
[70] J.r. Weiser, P.S. Shenkin, W.C. Still, Approximate atomic surfaces from linear combinations of pairwise overlaps (LCPO), J. Comput. Chem. 20 (1999) 217–230.
[71] W. Kabsch, C. Sander, Dictionary of protein secondary structure: pattern recognition of hydrogen-bonded and geometrical features, Biopolymers 22 (1983) 2577–2637.
[72] D.M. Walsh, D.J. Selkoe, A? Oligomers ? a decade of discovery, J. Neurochem. 101 (2007) 1172–1184.
[73] E.Y. Hayden, D.B. Teplow, Amyloid β-protein oligomers and Alzheimer's disease, Alzheimer's Res. Ther. 5 (2013) 60.
[74] I. Kuperstein, K. Broersen, I. Benilova, J. Rozenski, W. Jonckheere, M. Debulpaep, A. Vandersteen, I. Segers-Nolten, K. Van Der Werf, V. Subramaniam, D. Braeken, G. Callewaert, C. Bartic, R. D'Hooge, I.C. Martins, F. Rousseau, J. Schymkowitz, B. De Strooper, Neurotoxicity of Alzheimer's disease Aβ peptides is induced by small changes in the Aβ42 to Aβ40 ratio, EMBO J. 29 (2010) 3408–3420.
[75] M.M. Picken, G.A. Herrera, Thioflavin T Stain: an Easier and More Sensitive Method for Amyloid Detection, 2012, pp. 187–189.
[76] C. Di Natale, P.L. Scognamiglio, R. Cascella, C. Cecchi, A. Russo, M. Leone, A. Penco, A. Relini, L. Federici, A. Di Matteo, F. Chiti, L. Vitagliano, D. Marasco, Nucleophosmin contains amyloidogenic regions that are able to form toxic aggregates under physiological conditions, Faseb. J. 29 (2015) 3689–3701.
[77] A. Monji, H. Utsumi, T. Ueda, T. Imoto, I. Yoshida, S. Hashioka, K.-i. Tashiro, N. Tashiro, The relationship between the aggregational state of the amyloid-β peptides and free radical generation by the peptides, J. Neurochem. 77 (2001) 1425–1432.
[78] B. Guivernau, J. Bonet, V. Valls-Comamala, M. Bosch-Morato, J.A. Godoy, N. C. Inestrosa, A. Peralvarez-Marin, X. Fernandez-Busquets, D. Andreu, B. Oliva, F. J. Munoz, Amyloid-beta peptide nitrotyrosination stabilizes oligomers and enhances NMDAR-mediated toxicity, J. Neurosci. 36 (2016) 11693–11703.
[79] S.A. Kotler, J.R. Brender, S. Vivekanandan, Y. Suzuki, K. Yamamoto, M. Monette, J. Krishnamoorthy, P. Walsh, M. Cauble, M.M. Holl, E.N. Marsh, A. Ramamoorthy, High-resolution NMR characterization of low abundance oligomers of amyloid-beta without purification, Sci. Rep. 5 (2015) 11811.
[80] J. Guo, W. Sun, L. Li, F. Liu, W. Lu, Brazilin inhibits fibrillogenesis of human islet amyloid polypeptide, disassembles mature fibrils, and alleviates cytotoxicity, RSC Adv. 7 (2017) 43491–43501.
[81] B. Cheng, X. Liu, H. Gong, L. Huang, H. Chen, X. Zhang, C. Li, M. Yang, B. Ma, L. Jiao, L. Zheng, K. Huang, Coffee components inhibit amyloid formation of human islet amyloid polypeptide in vitro: possible link between coffee consumption and diabetes mellitus, J. Agric. Food Chem. 59 (2011) 13147–13155.
[82] B. Cheng, H. Gong, X. Li, Y. Sun, X. Zhang, H. Chen, X. Liu, L. Zheng, K. Huang, Silibinin inhibits the toxic aggregation of human islet amyloid polypeptide, Biochem. Biophys. Res. Commun. 419 (2012) 495–499.
[83] F.L. Palhano, J. Lee, N.P. Grimster, J.W. Kelly, Toward the molecular mechanism (s) by which EGCG treatment remodels mature amyloid fibrils, J. Am. Chem. Soc. 135 (2013) 7503–7510.
[84] C. Di Natale, S. La Manna, C. Avitabile, D. Florio, G. Morelli, P.A. Netti, D. Marasco, Engineered β-hairpin scaffolds from human prion protein regions: structural and functional investigations of aggregates, Bioorg. Chem. 96 (2020) 103594.

[85] C. Di Natale, S. La Manna, A.M. Malfitano, S. Di Somma, D. Florio, P. L. Scognamiglio, E. Novellino, P.A. Netti, D. Marasco, Structural insights into amyloid structures of the C-terminal region of nucleophosmin 1 in type A mutation of acute myeloid leukemia, Biochim. Biophys. Acta Protein Proteonomics 1867 (2019) 637–644.
[86] D. Florio, A.M. Malfitano, S. Di Somma, C. Mugge, W. Weigand, G. Ferraro, I. Iacobucci, M. Monti, G. Morelli, A. Merlino, D. Marasco, Platinum(II) O,S complexes inhibit the aggregation of amyloid model systems, Int. J. Mol. Sci. 20 (2019).
[87] Iacobucci Florio, Mansour Ferraro, Monti Morelli, Marasco Merlino, Role of the metal center in the modulation of the aggregation process of amyloid model systems by square planar complexes bearing 2-(2'-pyridyl)benzimidazole ligands, Pharmaceuticals 12 (2019) 154.
[88] P.L. Scognamiglio, C. Di Natale, M. Leone, R. Cascella, C. Cecchi, L. Lirussi, G. Antoniali, D. Riccardi, G. Morelli, G. Tell, F. Chiti, D. Marasco, Destabilisation, aggregation, toxicity and cytosolic mislocalisation of nucleophosmin regions associated with acute myeloid leukemia, Oncotarget 7 (2016) 59129–59143.
[89] S. La Manna, P.L. Scognamiglio, V. Roviello, F. Borbone, D. Florio, C. Di Natale, A. Bigi, C. Cecchi, R. Cascella, C. Giannini, T. Sibillano, E. Novellino, D. Marasco, The acute myeloid leukemia-associated Nucleophosmin 1 gene mutations dictate amyloidogenicity of the C-terminal domain, FEBS J. 286 (12) (2019 Jun) 2311–2328, https://doi.org/10.1111/febs.14815.
[90] M. Poletto, M.C. Malfatti, D. Dorjsuren, P.L. Scognamiglio, D. Marasco, C. Vascotto, A. Jadhav, D.J. Maloney, D.M. Wilson 3rd, A. Simeonov, G. Tell, Inhibitors of the apurinic/apyrimidinic endonuclease 1 (APE1)/nucleophosmin (NPM1) interaction that display anti-tumor properties, Mol. Carcinog. 55 (2016) 688–704.
[91] M. Chu, X. Chen, J. Wang, L. Guo, Q. Wang, Z. Gao, J. Kang, M. Zhang, J. Feng, Q. Guo, B. Li, C. Zhang, X. Guo, Z. Chu, Y. Wang, Polypharmacology of berberine based on multi-target binding motifs, Front. Pharmacol. 9 (2018).
[92] L.S. Cheng, R.E. Amaro, D. Xu, W.W. Li, P.W. Arzberger, J.A. McCammon, Ensemble-based virtual screening reveals potential novel antiviral compounds for avian influenza neuraminidase, J. Med. Chem. 51 (2008) 3878–3894.
[93] B.-k. Shin, S. Saxena, Substantial contribution of the two imidazole rings of the His13−His14 dyad to Cu(II) binding in amyloid-β(1−16) at physiological pH and its significance, J. Phys. Chem. 115 (2011) 9590–9602.
[94] S.L. Bernstein, N.F. Dupuis, N.D. Lazo, T. Wyttenbach, M.M. Condron, G. Bitan, D. B. Teplow, J.-E. Shea, B.T. Ruotolo, C.V. Robinson, M.T. Bowers, Amyloid-β protein oligomerization and the importance of tetramers and dodecamers in the aetiology of Alzheimer's disease, Nat. Chem. 1 (2009) 326–331.
[95] A.T. Petkova, Y. Ishii, J.J. Balbach, O.N. Antzutkin, R.D. Leapman, F. Delaglio, R. Tycko, A structural model for Alzheimer's -amyloid fibrils based on experimental constraints from solid state NMR, Proc. Natl. Acad. Sci. Unit. States Am. 99 (2002) 16742–16747.
[96] Y. Xiao, B. Ma, D. McElheny, S. Parthasarathy, F. Long, M. Hoshi, R. Nussinov, Y. Ishii, Aβ(1–42) fibril structure illuminates self-recognition and replication of amyloid in Alzheimer's disease, Nat. Struct. Mol. Biol. 22 (2015) 499–505.
[97] L. Gremer, D. Scholzel, C. Schenk, E. Reinartz, J. Labahn, R.B.G. Ravelli, M. Tusche, C. Lopez-Iglesias, W. Hoyer, H. Heise, D. Willbold, G.F. Schroder, Fibril structure of amyloid-beta(1-42) by cryo-electron microscopy, Science 358 (2017) 116–119.
[98] D.M. Walsh, D.M. Hartley, Y. Kusumoto, Y. Fezoui, M.M. Condron, A. Lomakin, G. B. Benedek, D.J. Selkoe, D.B. Teplow, Amyloid β-protein fibrillogenesis, J. Biol. Chem. 274 (1999) 25945–25952.
[99] A.K. Paravastu, R.D. Leapman, W.M. Yau, R. Tycko, Molecular structural basis for polymorphism in Alzheimer's -amyloid fibrils, Proc. Natl. Acad. Sci. Unit. States Am. 105 (2008) 18349–18354.
[100] R.H. Olsen, G. DeBusscher, W.R. McCombie, Development of broad-host-range vectors and gene banks: self-cloning of the Pseudomonas aeruginosa PAO chromosome, J. Bacteriol. 150 (1982) 60–69.
[101] T. Watanabe-Nakayama, K. Ono, M. Itami, R. Takahashi, D.B. Teplow, M. Yamada, High-speed atomic force microscopy reveals structural dynamics of amyloid β1–42 aggregates, Proc. Natl. Acad. Sci. Unit. States Am. 113 (2016) 5835–5840.
[102] S. Zhang, K. Iwata, M.J. Lachenmann, J.W. Peng, S. Li, E.R. Stimson, Y.a. Lu, A. M. Felix, J.E. Maggio, J.P. Lee, The alzheimer's peptide Aβ adopts a collapsed coil structure in water, J. Struct. Biol. 130 (2000) 130–141.
[103] M.G. Krone, L. Hua, P. Soto, R. Zhou, B.J. Berne, J.-E. Shea, Role of water in mediating the assembly of alzheimer amyloid-β Aβ16−22 protofilaments, J. Am. Chem. Soc. 130 (2008) 11066–11072.
[104] J. Hu, H. Sun, H. Hao, Q. Zheng, Prediction of fibril formation by early-stage amyloid peptide aggregation, J. Pharma. Anal. 10 (2020) 194–199.
[105] S. Giorgetti, C. Greco, P. Tortora, F. Aprile, Targeting amyloid aggregation: an overview of strategies and mechanisms, Int. J. Mol. Sci. 19 (2018) 2677.
[106] T.T.M. Thu, N.T. Co, L.A. Tu, M.S. Li, Aggregation rate of amyloid beta peptide is controlled by beta-content in monomeric state, J. Chem. Phys. 150 (2019) 225101.
[107] A.J. Modler, K. Gast, G. Lutsch, G. Damaschun, Assembly of amyloid protofibrils via critical oligomers—a novel pathway of amyloid formation, J. Mol. Biol. 325 (2003) 135–148.